Statistical Analysis of Wind Power Forecast Error

Hans Bludszuweit, José Antonio Domínguez-Navarro, *Member, IEEE*, and Andrés Llombart

***Abstract*—Wind power forecast error usually has been assumed to have a near Gaussian distribution. With a simple statistical analysis, it can be shown that this is not valid. To obtain a more appropriate probability density function (pdf) of the wind power forecast error, an indirect algorithm based on the Beta pdf is proposed. Measured one-year time series from two different wind farms are used to generate the forecast data. Three different forecast scenarios are simulated based on the persistence approach. This makes the results comparable to other forecast methods. It is found that the forecast error pdf has a variable kurtosis ranging from 3 (like the Gaussian) to over 10, and therefore it can be categorized as fat-tailed. A new approximation function for the parameters of the Beta pdf is proposed because results from former publications could not be confirmed. Besides, a linear approximation is developed to describe the relationship between the persistence forecast and the related mean measured power. An energy storage system (ESS), which reduces the forecast error and smooths the wind power output, is considered. Results for this case show the usefulness of the proposed forecast error pdf for finding the optimum rated ESS power.**

***Index Terms*—Error analysis, forecasting, wind, wind power generation.**

I. Introduction

THE increasing penetration of wind power in the electricity grids leads to the need of a better understanding of the wind power forecast error and if possible, its reduction. Obviously, with rising penetration levels, the impact of wind generation on the electrical energy system must be taken into account [1]. Although embedded wind generation can be positive for a weak grid [2], it can also lead to instabilities [3]. To avoid such instabilities, the system reserve has to be increased [4] or sometimes, important amounts of wind energy must be dumped [5]. Though forecast error does not only have technical but it also has economical aspects. Unforeseen energy generation will cause additional costs, especially when wind energy is traded in short-term energy markets [6]–[8]. In [6] it is stated that prediction error costs can reach as much as 10% of the total incomes from generated energy.

An option to increase the system reserve (or spinning reserve) to deal with the forecast error may be an energy storage system (ESS). Placing such an installation near the wind generator has a number of very benign effects on the energy system. In [9] a good introduction is given about possible applications of energy storage in relation to high wind penetration in weak grids. In this context, ESS can be categorized as proposed in [9] by their typical run times, applications and energy sizes as shown in Table I.

TABLE I
Typical Run Times and Applications of Energy Storage Systems [9]

Run time	Application	Energy capacity
Seconds	Voltage stabilization	kWh
Minutes	Output smoothing Stabilizing weak grids	several MWh
Hours	Renewable energy time shifting Ancillary services (spinning reserve)	> 10 MWh

The typical runtime is obtained by dividing the energy capacity by the rated power, which is usually in the megawatt range.

The benefits of energy storage in the range of seconds are shown in [10], while in [11] the economical benefits of a water storage (hours of runtime) combined with wind generation are shown. In [12] a method is presented to schedule energy storage for wind power plants in the electricity markets using time-step simulation for the ESS sizing. A probabilistic method for storage sizing is proposed in [13], applying spectral analysis of the intermittent renewable generation.

In this work, the forecast error pdf is studied because it can give important information for short-term trading in energy markets or even for the optimal sizing of rated ESS power.

In the literature we can find very few works about wind power forecast error distributions. The relationship of the statistical behavior of the forecast error and ESS sizing is mentioned in [4] and [6]–[8], but little emphasis is given to the actual wind power forecast error pdf. In [7] histograms from measured time series are used for the forecast error description and a standard distribution is assumed in [4] and [11]. In [14] the uncertainty of wind power forecasts is quantified using the well-known distribution of wind speed forecasts in conjunction with the power curve of the wind energy conversion system (WECS).

The difficulty in finding a proper definition for the forecast error pdf lies in the great variety of its shape depending on the forecast horizon and method. It is shown in this paper that the error pdf is fat-tailed with variable kurtosis. Therefore, it cannot be modeled with the normal distribution.

In the present study, an alternative method based on [15] is adopted to obtain a more suitable forecast error pdf. The method consists in dividing the forecast into 50 power classes or bins and modeling the distribution of measured power within each forecast bin with the Beta pdf. The higher number of 50 bins, compared to only four bins in [15], leads to new findings for the parameters of the Beta pdf. Given the power pdf associated to each bin, the forecast error pdf can be obtained. It is found that the Beta distribution gives reasonably accurate results. However, further investigation on alternative distributions may improve these results.

The paper is organized as follows. In Section II the steps of the proposed method are explained and in Section III results for the forecast error pdf and ESS sizing are presented. The obtained

Manuscript received August 7, 2007; revised December 7, 2007. This work was supported by the CIRCE foundation. Paper no. TPWRS-00558-2007.

The authors are with the Electrical Engineering Department, University of Zaragoza, and also with the CIRCE foundation, associated with it, Zaragoza, Spain (e-mail: hblud@unizar.es; jadona@unizar.es; llombart@unizar.es).

Digital Object Identifier 10.1109/TPWRS.2008.922526

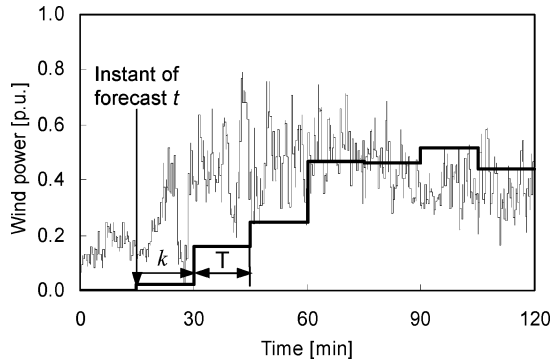

Fig. 1. Wind power time series (thin line) with persistence forecast (bold line), forecast delay k, and prediction time interval T ($T = k = 15$ min).

forecast error pdf is used to optimize the rated ESS power under given constraints and it is found that, in some cases, it can be more than 80% lower than the installed wind power.

II. Methodology

In Section II-A, a method is shown for simulating different forecast qualities or scenarios. In Section II-B, the forecast error is found to be fat-tailed with variable kurtosis and some possible distributions are discussed. The application of the Beta pdf is developed in Section II-C, where a new, nonlinear function is proposed for the approximation of the parameters standard deviation σ and mean value μ. In Section II-D the relationship between the persistence forecast and the mean measured power related to this forecast is discussed and the findings in [16] could be verified. In Section II-E the calculation of the total forecast error distribution is explained and finally in Section II-F the procedure to obtain the energy loss as a function of nominal ESS power is shown.

A. Modeling Forecast Scenarios Using Persistence

We have analyzed several one-year time series of generated wind power from two sites. The two datasets will be called A and B. In dataset A, 10 min means from 32 different wind generators from the same wind farm were aggregated, so that a database of around 1 million values was available for statistical analysis. In dataset B, 15 min means were available for three spatially very close wind farms, with around 100 000 data values.

In the world of wind power forecast exist a huge variety of different forecast methods. But every method has to be compared always with the simplest one: the persistence forecast. Therefore, this simple approach was chosen to simulate three different scenarios of forecast quality. This allows us to investigate the changes in the error distribution with changing forecast scenario. For better understanding of the persistence method used here, in Fig. 1 a measured wind power time series (thin line) and the persistence forecast (step function, bold line) are depicted for a dataset of 1 second mean wind power. The instant t is shown when the forecast is done and the forecast time interval width T, where the mean wind power is predicted. This time interval has to start later than t, so that a forecast delay k has to be defined.

This delay describes the time gap between the instant, when the forecast is done and the beginning of T. In short-term energy markets k is termed market closure delay [8].

In Fig. 1, the mean wind power obtained from time interval [0,15] is the forecast for the interval [30,45]. Therefore, it can be stated that the persistence forecast in this case is 2T time-shifted relative to the interval, where the mean value was calculated. According to the nomenclature proposed in [17], the persistence forecast can be written as

$$\hat{P}(t+k\,|t) = \frac{1}{T}\sum_{i=0}^{n-1} P(t - i\Delta t) \tag{1}$$

where $\hat{P}(t+k|t)$ is the wind power forecast for time $t+k$ made at time origin t, k the prediction horizon, T the prediction interval length (here $T = k$), $P(t - i\Delta t)$ the measured wind power for time t and the previous i time steps within T, n the number of time steps within T and Δt the time step length of the measured time series ($T = n\Delta t$).

In the following, three forecast scenarios are defined. This way, the impact of the forecast model is simulated without using a specific forecast model. If a forecast model is determined, it can be classified according to the scenarios.

The worst-case scenario, termed $T\times 2$, is based on a persistence forecast with $k = T$. The forecast is only updated once for each prediction interval, so the forecast value is constant during the whole prediction interval T, as shown in Fig. 1. This is the worst case because no forecast model should perform worse than this.

The $T\times 1$ scenario is simulating an intermediate case. The calculated mean value of each interval is shifted in time by the width of prediction interval T. This is equal to a persistence forecast with $k = 0$, which means an important improvement in comparison with the scenario $T\times 2$.

The best-case scenario, termed $T\times 0$, is obtained by assigning the measured mean value in the interval T as forecast for the same interval ($k = -T$). This way, a perfect forecast of the mean value for each interval is simulated. The error only consists in the power fluctuations within the interval T.

The normalized prediction error ε is calculated as the difference between two time series of the same length. Following [17], it can be written as follows:

$$\varepsilon(t+k\,|t) = P(t+k) - \hat{P}(t+k\,|t) \tag{2}$$

where k is the prediction delay, $\hat{P}(t+k|t)$ is the wind power forecast for time $t+k$ for the prediction made at the origin t and P is the measured wind power.

B. Evaluating Possible Distributions of the Forecast Error

As it will be shown, the tail of the error pdf is of special interest for the ESS sizing. Therefore, kurtosis was chosen as the statistical parameter to evaluate the tail of the studied pdf. The kurtosis κ of a distribution of zero mean random variable ε is defined via

$$\kappa = \frac{E\left(\varepsilon^4\right)}{\sigma^4} \tag{3}$$

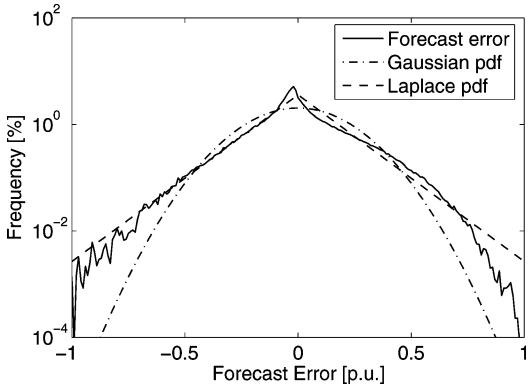

Fig. 2. Comparison of a histogram of 24-h forecast error data (kurtosis 4.8) with Gaussian and Laplace pdf having the same standard deviation as the forecast error.

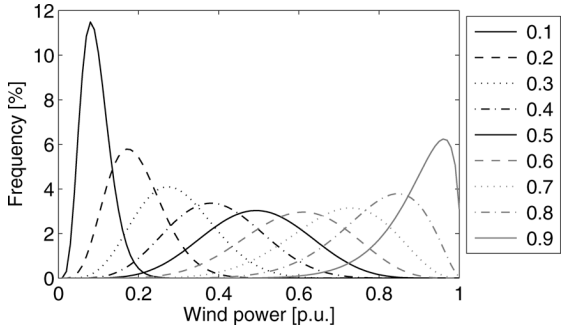

Fig. 3. Approximated Beta pdf of measured wind power for nine different forecast power classes.

where E denotes the expectation operator and σ the standard deviation.

If κ is larger than 3 (the value associated to normal distribution), the distribution is called leptokurtic or fat-tailed. By calculating the kurtosis of the forecast error data, it can be shown that the normal pdf is not appropriate. In fact persistence forecast errors show values of κ above 10 (forecast below 1 h) and even below 3 (beyond 24 h), which means that the observed distributions in general are leptokurtic.

In Fig. 2 the histogram of an example of 24-h forecast data with a kurtosis of 4.8 is shown. In the same plot the Gaussian and Laplace pdf are depicted, which have the same standard deviation as the sample data. The Laplace pdf (with $\kappa = 6$) was chosen as an example of fat-tailed distributions. As expected, the tail of the forecast error pdf is situated between the Gaussian and the Laplace pdf, being $3 < \kappa < 6$.

As mentioned above, the kurtosis of the error ranges from below 3 to above 10, indicating a considerable variation across the different forecast horizons. The two exposed distributions show a fixed value of κ. There are well-known distributions with variable kurtosis, but up to now, no distributions have been proposed to model the forecast error, except the normal. Therefore, in this paper an indirect approach using the Beta distribution is applied based on assumptions made in [15] as it is described in Section II-C.

The kurtosis of Beta pdf is variable and is calculated as in the following (see [18]):

$$\kappa_{beta} = 6 \cdot \frac{\alpha(\alpha+1)(\alpha+2\beta) + \beta(\beta+1)(\beta+2\alpha)}{\alpha\beta(\alpha+\beta+2)(\alpha+\beta+3)} + 3 \quad (4)$$

where α and β are the parameters of Beta pdf.

Besides its variable kurtosis, the advantage of Beta pdf consists of its simplicity (it is defined by only two parameters) and that its values are limited to the interval [0,1], as well as the normalized wind power.

C. Approximation of a Beta Pdf for Each Power Forecast Bin

The indirect approach, adopted to obtain the error pdf, is based on [15]. First, forecast results are sorted into power classes or bins and the distribution of the measured power within each forecast bin is assumed to follow a Beta pdf. Knowing the pdf associated to each forecast bin, the error pdf of this bin can be calculated. Adding up the error pdfs of all bins, the overall forecast error pdf can be obtained.

Therefore, the forecast time series are generated as described in Section II-A and every forecast is assigned to a measured wind power value. Then the data pairs [measured, forecast] are sorted by the forecast values and assigned to forecast power bins. The bin width must be chosen depending on the number of data available. In this case 50 bins with 0.02 p.u. bin width seem to be a good choice, but if the database is smaller, the number of bins must be reduced.

It is assumed that all measured values of one forecast bin have the same forecast $P_{p,i}$, which is the mean value of all the calculated forecasts corresponding to bin i. The distribution within bin i is called $pdf(P)_i$. The Beta pdf is given by the following equations:

$$pdf(P) = \frac{P^{\alpha-1} \cdot (1-P)^{\beta-1}}{B(\alpha,\beta)} \quad (5)$$

$$B(\alpha,\beta) = \int_0^1 P^{\alpha-1} \cdot (1-P)^{\beta-1}\, dP \quad (6)$$

where P is the measured wind power per unit (p.u.), α and β are the parameters and $B(\alpha,\beta)$ is the Beta function.

As can be seen in (6), Beta function $B(\alpha,\beta)$ is simply the integral of the term in the numerator of (5), which normalizes the integral of $pdf(P)$ in the interval [0,1]. Therefore in [15], the following form was chosen to represent Beta pdf:

$$pdf(P) = P^{\alpha-1} \cdot (1-P)^{\beta-1} \cdot n \quad (7)$$

where n is the normalization factor $1/B(\alpha,\beta)$.

In Fig. 3 an example is given for a possible result of approximated wind power $pdf(P)_i$ for nine different predicted power classes i with mean forecast $P_{p,i}$.

As mentioned in [6], the parameters α and β are related to the parameters σ^2 (variance) and μ (mean). The following equations show these relationships:

$$\mu = \frac{\alpha}{\alpha+\beta} \quad (8)$$

$$\sigma^2 = \frac{\alpha \cdot \beta}{(\alpha+\beta+1) \cdot (\alpha+\beta)^2.} \quad (9)$$

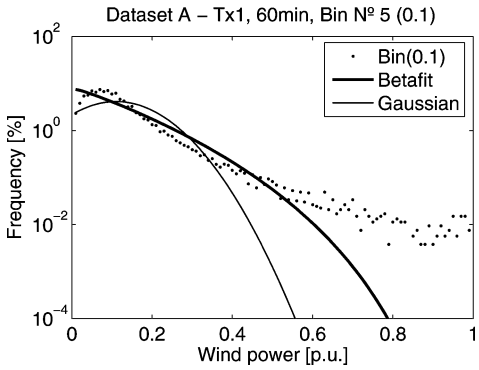

Fig. 4. Comparison of the histogram of measured wind power (dots) with Beta pdf (bold solid) and normal pdf (solid); forecast power bin: 5 of 50 (forecast: 0.1 p.u.).

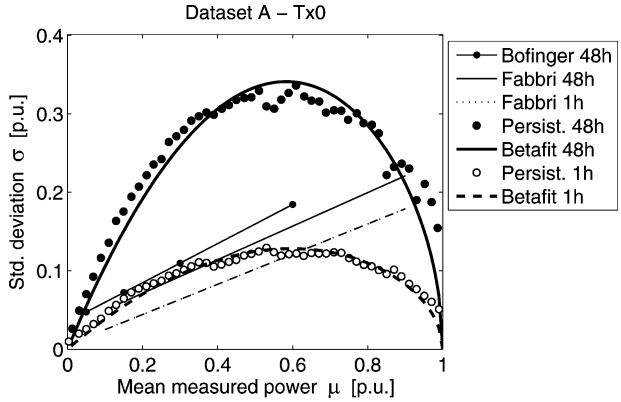

Fig. 5. Two examples for the approximation of parameter pairs (μ, σ) from persistence forecast together with curves from Bofinger [15] and Fabbri [6]; Dataset A, $T\times 0$ forecast.

Equations (8) and (9) can be reversed to calculate α and β directly from μ and σ^2 as shown in

$$\alpha = \frac{(1-\mu)\cdot\mu^2}{\sigma^2} - \mu \tag{10}$$

$$\beta = \frac{1-\mu}{\mu}\cdot\alpha. \tag{11}$$

Next we show the advantages of using the Beta pdf in spite of the Gaussian pdf for approximating the forecast error distribution. As an example, in Fig. 4 the histogram of one forecast power bin is compared to the fitted Beta pdf and the corresponding Gaussian.

The distribution of data in this example bin is very fat-tailed with a kurtosis of around 17. The fitted Beta reaches around 5, which is significantly better than the normal pdf ($\kappa = 3$). In Fig. 4 this can be appreciated for wind powers above 0.5 p.u., where the normal pdf tends much faster to zero than the Beta. However, both tend much faster to zero than the actual measured data does. It should be mentioned that the Gaussian and Beta distributions in this example have the same values of μ and σ as the measured data.

The previous example showed that the tail of the wind power distribution cannot always be modeled perfectly with the Beta pdf. As a consequence, the purpose of this paper is to evaluate its performance, as no better pdf has been proposed yet in the literature.

After the approximation process, for every forecast bin i, parameter pairs $\{\alpha_i, \beta_i\}$ and $\{\mu_i, \sigma_i\}$ are obtained. As in [15], the $\{\mu, \sigma\}$ pair is chosen for the representation of the results. In Fig. 5 examples for 1-h and 48-h forecasts are shown in comparison with the curves published in [6] and [15]. A nonlinear behavior was observed in all the investigated forecast scenarios and prediction horizons, while in [6] and [15] a linear relationship between μ and σ is assumed. This nonlinearity can be explained with the power curve of WECS. As shown in [14], the first-order derivative of the power curve is directly proportional to the uncertainty of the power forecast. At zero and nominal power (1 p.u.) the derivative is near zero, while at around 0.5 p.u. it passes a maximum. The same can be observed for the standard deviation in Fig. 5.

The difference in results may be caused by the different procedures used to obtain the data. In [15], the forecast horizon k is 48 h with $T = 24$ h. Forecasts of one day mean values lead to statistical database of only 365 values. The bias correction, performed on this data, reduces the data further to 100 values. As this is a very poor amount of data, the linear approximation was based on only 4, non-equally distributed forecast bins. In [6] no information is given about how the linear approximation was obtained from the measured data. In the present work, 50 bins with equal bin widths were used. So possibly, the nonlinear behavior was not revealed in [15] for the lack of power bin resolution.

The higher standard deviation of the presented examples is due to the power fluctuations within the forecast interval which were not taken into account in [15]. Considering, for example, a 1-h forecast, in the present work the six corresponding 10-min measured values of this interval were used to obtain the standard deviation, while in [15], every forecast interval only has one forecast associated to the measured mean value.

The following equation is proposed as a new approximation function:

$$\sigma = \sqrt{\mu\cdot(1-\mu)\cdot(-p_2\cdot\mu^2 + p_1\cdot\mu)} \tag{12}$$

where p_1 and p_2 are the approximation parameters.

The curves named "Betafit" in Fig. 5 show two examples of this approximation. The special form of the function is due to the fact that the parameter α cannot be negative. From (10) follows (13) which shows clearly that σ^2 must be zero at the boundaries of the interval $\mu = [0, 1]$:

$$\alpha = \frac{(1-\mu)\cdot\mu^2}{\sigma^2} - \mu \geq 0 \Rightarrow (1-\mu)\cdot\mu \geq \sigma^2. \tag{13}$$

Therefore, it is practical to use the term $\mu\,(1-\mu)$ as a factor in the polynomial approximation of σ^2.

The analysis of different prediction horizons up to 30 days ($T = 720$ h) has shown that good results can be obtained with only two polynomial coefficients. The coefficient p_2 has a negative sign, in order to obtain positive values for p_1 and p_2.

In Fig. 6 coefficients are shown as a function of T for the three forecast scenarios. It can be observed that the two datasets show quite different behavior, although the global tendency is similar. This can be explained by the power curves as described

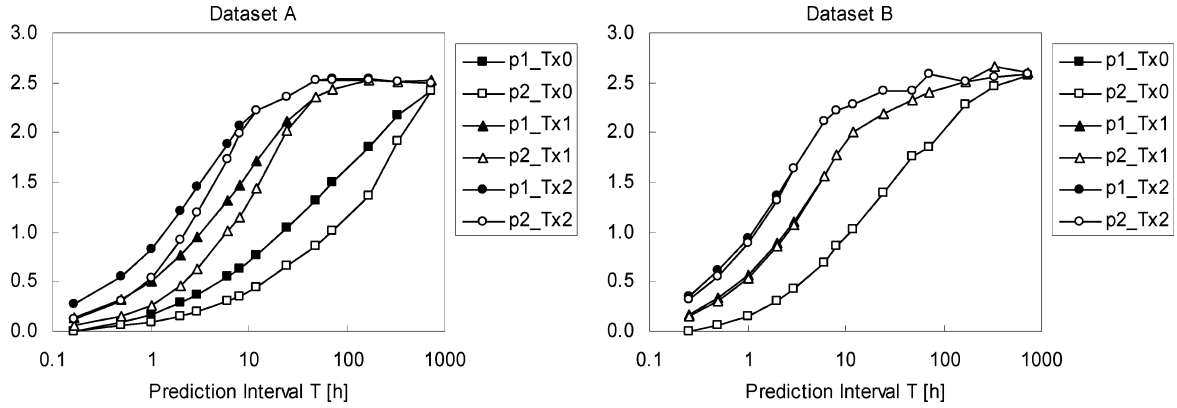

Fig. 6. Approximation parameters for fitting function $\sigma = f(\mu)$ as a function of prediction interval T and the three forecast scenarios ($T\times 0$, $T\times 1$, $T\times 2$) for datasets A and B.

in [14]. Dataset A was taken from constant speed while dataset B was taken from variable speed WECS.

Very interesting is that the coefficients in dataset B are almost identical. Equal values of p_1 and p_2 mean that the curve $\sigma(\mu)$ is symmetric. If the symmetric case is assumed, the approximation function can be simplified as expressed in (14). The only remaining parameter p can be calculated as the square root of the former parameters $p_1 = p_2$

$$\sigma = p \cdot \mu \cdot (1 - \mu). \tag{14}$$

Further investigation with more datasets is needed to evaluate if the assumption of symmetric $\sigma(\mu)$ is valid for variable wind turbines in general or if the case of dataset B is an exception.

D. Analysis of the Relationship Between Mean Power Forecast and Measured Power

In [6] and [15] σ_i within a forecast bin i is represented as a function of the mean predicted power $P_{p,i}$ of this bin. It must be noted that these values can only be interpreted directly as parameters of the Beta pdf if $P_{p,i}$ is equal to the mean measured power μ_i in this bin. Indeed in [6] and [15] $\mu_i = P_{p,i}$ is assumed, but without emphasizing that the parameter μ_i of the Beta pdf must be derived from the measured data, and not from the forecast data. In [15] a simple neuronal network is applied to correct the initial forecast with the aim to approach $\mu_i = P_{p,i}$, while in [6] it is only stated that the forecast will be "centered in the mean value." However, it will be shown now that this assumption is not valid for the persistence forecast.

If a linear relationship between P_p and μ is considered and it is further assumed that all curves cross the point of the long-term mean, the fitting function $\mu(P_p)$ can be written as in

$$\mu = m \cdot P_p + (1 - m) \cdot \overline{P} \tag{15}$$

where P_p is the mean forecast within a forecast bin, m is the slope of the linear fit, and $\overline{P}$ is the long-term mean.

As shown in Fig. 7, for short forecast horizons up to 1 h, $P_p = \mu$ is almost true, but not when the forecast horizon k becomes larger.

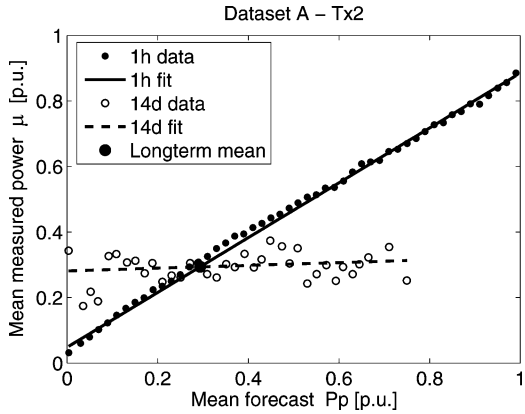

Fig. 7. Linear approximation of the mean forecast and measured mean within a forecast bin; examples for $T = 1$ h and 336 h (14 days) and $T\times 2$ scenario.

As it can be seen in Fig. 7, the slope m of the linear fit depends strongly on the forecast horizon T. While the linearity is maintained, the slope of the curve tends to zero for very large values of T. In fact, for the 14-day forecast, the mean value of measured power is almost constant for all forecasts and equal to the long-term mean (in this case the total mean of the entire dataset).

In Fig. 8 the linear approximations following (15) for several prediction intervals T are shown for the example of $T\times 2$ scenario using dataset A.

In other words, the long term mean value becomes the best forecast for large forecast horizons. Therefore, in [16] a modified persistence model is proposed as a new reference (cited also in [17] and [19]), which takes into account this effect. This new reference can be written as

$$\hat{P}_{NR}(t + k\,|t) = a_k \cdot \hat{P} + (1 - a_k) \cdot \overline{P} \tag{16}$$

where $\hat{P}_{NR}$ is the new reference forecast, a_k is the correlation coefficient between $P(t)$ and $P(t + k)$, $\hat{P}$ is the persistence forecast and $\overline{P}$ is the long-term mean.

Equations (15) and (16) have the same structure of a linear function, with the only difference that the slope in (15) is m and in (16) is the autocorrelation coefficient a. Using (15), slopes m

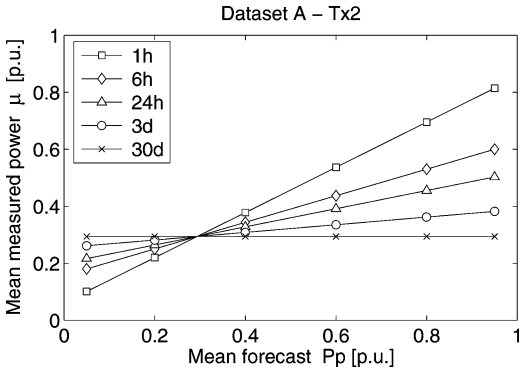

Fig. 8. Linear approximation for measured mean as a function of mean forecast within a forecast bin for several prediction intervals T; $T\times 2$ scenario, dataset A.

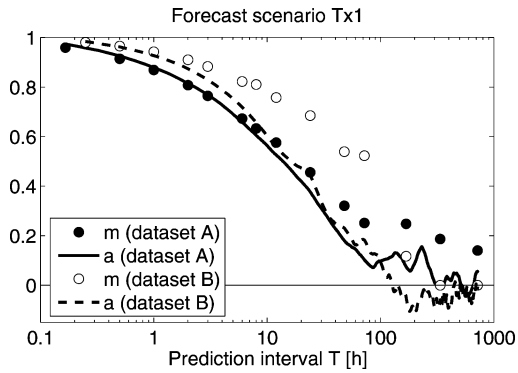

Fig. 9. Comparison of the autocorrelation coefficient "a" with slope "m" of the linear fit as a function of prediction interval T; forecast scenario $T\times 1$, datasets A and B.

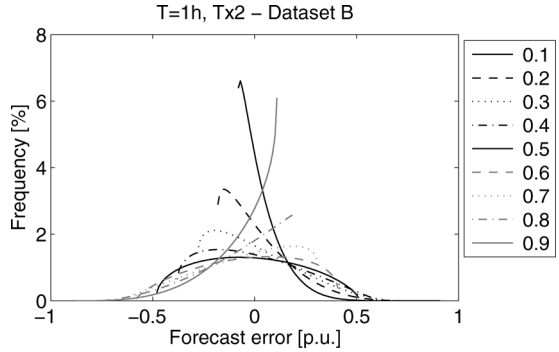

Fig. 10. Superposed forecast errors for nine different forecast power bins for a 1-h $T\times 2$ forecast using dataset B.

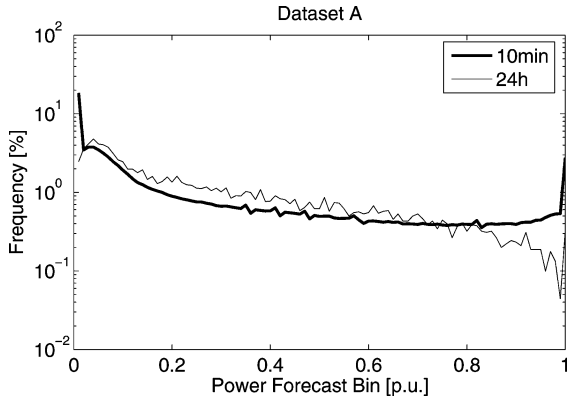

Fig. 11. Comparison of the frequencies in each forecast bin. "10 min" is the histogram (0.01 bin width) of the measured wind power of dataset A (10 min means); "24 h" is the histogram of the persistence forecast for a forecast time interval $T = 24$ h.

are calculated for all considered prediction intervals T. In Fig. 9 $m(k)$ and $a(k)$ for the two datasets and forecast scenario $T\times 1$ are shown. Results for $T\times 2$ are similar and m for $T\times 0$ must obviously be unity.

From Fig. 9 the similarity between m and a is confirmed, but also some differences can be found. While for small values of T the slope m is almost equal to the autocorrelation coefficient a, it is greater than a for higher values of T. This can be explained by the persistence forecast approach chosen in this work. For large values of T, the forecast is the average value over a large time interval. The autocorrelation does not take into account this averaging while m includes it. In dataset A, m is almost equal to a up to around $T = 10$ h, but in dataset B the similarity only holds up to $T = 2$ h. This can be due to the smaller database of dataset B (ten times smaller) which makes the calculation of m less reliable. But it is possible that this effect is also due to the individual behavior of the wind data, as, for example, the symmetry of $\sigma(\mu)$. Interestingly, the autocorrelation of dataset A and B is very similar, which shows that it is less sensible to the specific properties of the data available.

E. Obtaining the Forecast Error Pdf From the Beta Distributions

Knowing the pdf of the measured wind power within every forecast bin, the error distribution of each bin can be obtained easily by subtracting the mean predicted power of the bin from the amplitude axis of the pdf. The result for nine of the 50 bins chosen in this case can be seen in Fig. 10.

Once the pdf of the forecast error is known for all bins, the total forecast error pdf can be calculated by adding up the pdfs of all bins. The pdf for each bin is normalized to 100%, though the sum must be weighted. The weight w of each bin is equal to the probability that a forecast belongs to it. Weighting the sum is necessary because the probability that a forecast belongs to the 0.1-p.u. bin may be ten times higher than it is for the 0.9-p.u. bin. The weighted sum can be written as in

$$pdf\,(\varepsilon) = \sum_{i=1}^{n} w\,(i)\cdot pdf\,(\varepsilon_i) \tag{17}$$

where $pdf(\varepsilon)$ is the total forecast error pdf, i the bin number, n the total number of bins, $w(i)$ the forecast power bin weight function and $pdf(\varepsilon_i)$ the forecast error pdf in bin i.

The weight function $w(i)$, representing the weight of each bin, is a histogram with n bins of long-term forecast data. The histogram depends strongly on the forecast interval length T as shown in Fig. 11. The frequency values of 10-min and 24-h forecast data for the bins from 0.8 to 1 p.u. differ by a factor 10 or more.

It should be noted that the histogram obtained from the persistence forecast is representative for any forecast method, because

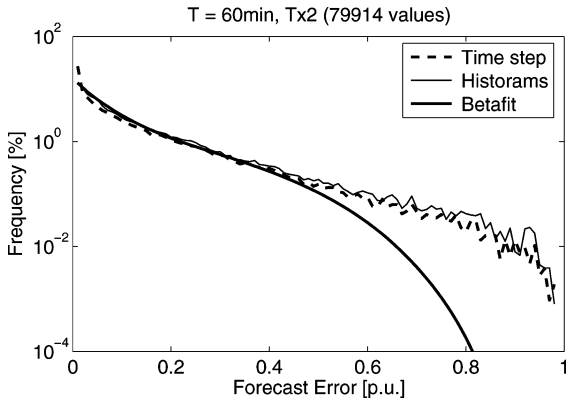

Fig. 12. Comparison of the real error distribution obtained from time-step simulation (dashed) from the histograms of each bin (solid) and using the Beta pdf (bold solid); 1-h $T\times 2$ forecast, dataset B.

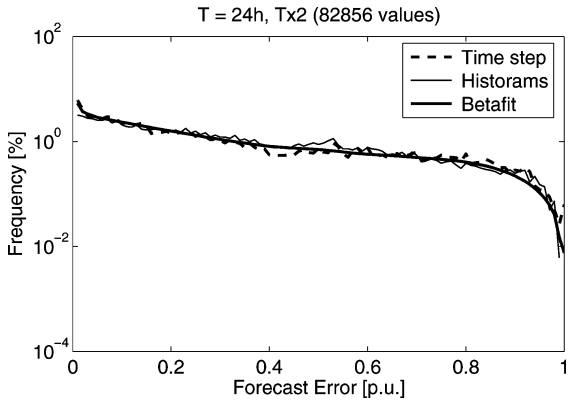

Fig. 13. Comparison of the real error distribution obtained from time-step simulation (dotted) from the histograms of each bin (solid) and using the Beta pdf (bold solid); 24-h $T\times 2$ forecast, dataset B.

the pdf of the mean values of generated power in time intervals equal to T and the predicted power should be always the same.

F. Calculating Energy Loss as a Function of ESS Power

Once the forecast error pdf is known, the energy loss of an energy storage system designed to reduce the forecast error can be calculated. If the energy loss is a function of the nominal power of the ESS, the sizing depends only on the allowed energy loss, termed rejection limit L.

If $pdf(\varepsilon)$ is the probability density function of the forecast error ε and P_{ESS} the nominal power of the ESS, the rejection limit L can be calculated as follows:

$$L = \frac{1}{\overline{P}} \int_{P_{ESS}}^{1} pdf\,(\varepsilon) \cdot (\varepsilon - P_{ESS})\, d\varepsilon. \tag{18}$$

When $pdf(\varepsilon)$ is given in [%] and ε in [p.u.], the integral in (18) represents the energy loss in percent of the multiplication of the installed power P_{inst} with 8760 h. In order to get energy loss as percent of the total generated energy, the integral has to be divided by the long-term mean $\overline{P}$ in [p.u.].

From (18) it can be seen that energy loss L is proportional to the integral of the tail of the pdf, starting from P_{ESS} up to 1. Therefore, to obtain satisfying results, the pdf must be especially precise in its tail region.

III. Results

The forecast error pdf by itself is an important result of this study. Examples are shown and its accuracy is discussed. The second result consists in the application of the error pdf. Sizing results are validated by a time-step method with the same numerical inputs.

A. Forecast Error Pdf From Beta Distributions

As mentioned before, the tail of the error pdf is of special relevance to this study. Therefore, all results are shown in semi-logarithmic plots for a better visibility of the tail region. The proposed algorithm is validated by using the histogram of measured data in every forecast bin instead of the approximated pdf, as it should give the same result as the time-step analysis. In Figs. 12 and 13, three curves are shown as the result of the time-step method (dashed line), using the histogram (thin solid line) and using the Beta pdf (bold solid line).

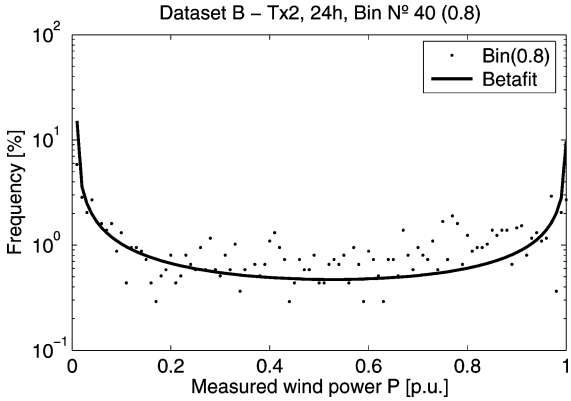

Fig. 14. Fitting the wind power distribution of a 24-h $T\times 2$ forecast in forecast bin 0.8 p.u.; dataset B.

In the example in Fig. 12, the Beta distribution is not able to model the fat tail of the forecast error. In Fig. 13 results for a 24-h forecast are shown. Here, the algorithm performs very well because it is able to approximate unexpected distributions like it is shown in Fig. 14.

B. ESS Nominal Power as a Function of Energy Rejection Limit

Thinking of the ESS sizing process, the first step is defining the nominal power of ESS termed P_{ESS}. The first guess for P_{ESS} is the installed wind power. But as already demonstrated, large power errors are rare and if a certain energy loss is allowed, nominal power of storage can be reduced. So the selection criterion for P_{ESS} is to maintain energy loss $L(P_{ESS})$ below the previously established maximum limit L_0. This limit can be found from the trade-off between the investment in the ESS and the forecast error cost.

Further work has to be done to determine this maximum limit properly.

To illustrate the usefulness and the limitations of the obtained pdf, P_{ESS} has been calculated for the two datasets under the

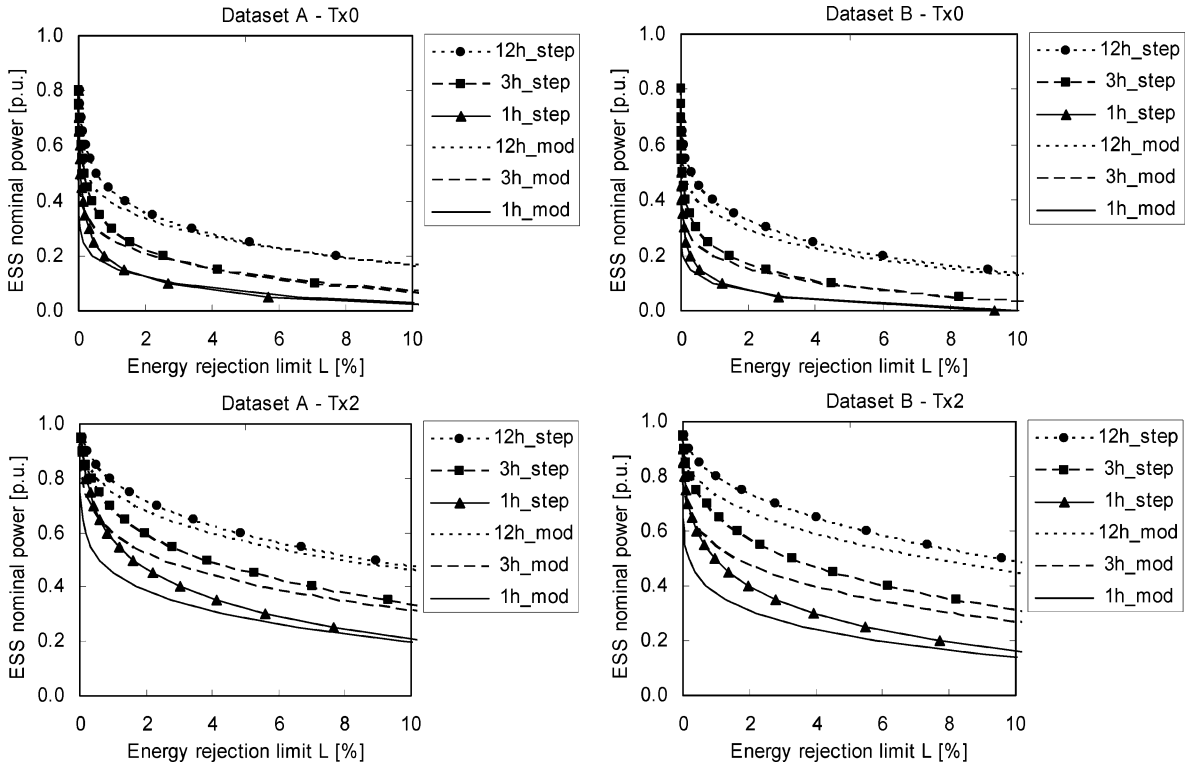

Fig. 15. Minimum ESS nominal power as a function of permitted energy rejection; comparison of time step calculation ("step") and statistical model ("mod") for datasets A and B and forecast scenarios $T\times 0$ and $T\times 2$.

three forecast scenarios $T\times 0$, $T\times 1$ and $T\times 2$. The results for $T\times 0$ and $T\times 2$ are shown in Fig. 15. As it could be expected, the best-case scenario $T\times 0$ permits lowest values of P_{ESS}. Considering a 1-h forecast and an energy rejection L of 2% of the total generated energy, P_{ESS} would be around 15% of the installed wind power P_{inst} for dataset A and below 10% in case of dataset B.

P_{ESS} increases with forecast horizon and reaches about 30%–35% of P_{inst} for the 12-h forecast. On the other hand, P_{ESS} is higher if the forecast quality is worse. Given $L = 2\%$, for a $T\times 2$ 1-h forecast, a reduction of P_{ESS} to about 40%–45% of the P_{inst} can be achieved, and 70%–75% for a 12-h forecast.

Compared to time step simulation, Fig. 15 shows that in all cases P_{ESS} is underestimated, especially for small rejection limits. This is caused by too small kurtosis of the Beta pdf. In general it can be stated that the proposed algorithm performs well for values of L greater than 2% for both datasets.

It must be noted that the forecast error pdf has been used to define only the ESS power. Without energy capacity as second parameter, the ESS sizing is not complete. Ongoing work is done to obtain a probabilistic description for energy capacity as well.

IV. Conclusions

A new, indirect method has been developed to obtain a probability density function of wind power forecast error. Important discrepancies with former publications were found by analyzing the relationship of mean and standard deviation of the measured wind power depending on the forecast. No linearity could be found and a polynomial approximation is proposed. The relationship between mean measured wind power and mean persistence forecast was found to be related to the autocorrelation coefficient.

The Beta pdf was chosen to describe the error, because it models well the distribution of wind power given a certain forecast. One important advantage of the Beta pdf is its variable kurtosis, which makes it more suitable than the normal pdf to model the fat-tailed forecast error distribution observed. But even though, it should be mentioned that for forecasts up to 24 h, Beta pdf is not fat-tailed enough. This leads to an underestimation of the frequency of the largest errors and in consequence to an underestimation of the ESS power needed to eliminate the forecast error.

As a result of this work, important improvements have been achieved for an existing approach which already has been used in other publications.

The determination of the ESS power as a function of the expected forecast error is a powerful tool in the task of ESS sizing for power systems. Further work is done to complete the study with a similar analysis for the ESS energy capacity and finally an economic optimization algorithm.

References

[1] J. G. Slootweg, "Wind power—Modelling and impact on power system dynamics," Ph.D., Tech. Univ. Delft, Delft, The Netherlands, 2003.
[2] T. Ackermann, K. Garner, and A. Gardiner, "Embedded wind generation in weak grids – Economic optimisation and power quality simulation," *Renewab. Energy*, vol. 18, pp. 205–221, 1999.
[3] J. O. G. Tande, "Exploitation of wind-energy resources in proximity to weak electric grids," *Appl. Energy*, vol. 65, pp. 395–401, 2000.
[4] R. Doherty and M. O'Malley, "A new approach to quantify reserve demand in systems with significant installed wind capacity," *IEEE Trans. Power Syst.*, vol. 20, no. 2, pp. 587–595, May 2005.

[5] J. K. Kaldellis, K. A. Kavadias, A. E. Filio, and S. Garofallakis, "Income loss due to wind energy rejected by the Crete island electrical network—The present situation," *Appl. Energy*, vol. 79, pp. 127–144, 2004.
[6] A. Fabbri, T. G. S. Román, J. R. Abbad, and V. H. M. Quezada, "Assessment of the cost associated with wind generation prediction errors in a liberalized electricity market," *IEEE Trans. Power Syst.*, vol. 20, no. 3, pp. 1440–1446, Aug. 2005.
[7] P. Pinson, C. Chevalier, and G. Kariniotakis, "Optimizing benefits from wind power partisipation in electricity markets using advanced tools for wind power forecasting and uncertainty assessment," in *Proc. 2004 EWEC'04*, London, U.K..
[8] G. N. Bathurst, J. Weatherill, and G. Strbac, "Trading wind generation in short term energy markets," *IEEE Trans. Power Syst.*, vol. 17, no. 3, pp. 782–789, Aug. 2002.
[9] J. McDowall, "Integrating energy storage with wind power in weak electricity grids," *J. Power Sources*, vol. 162, no. 2, pp. 959–964, Nov. 2006.
[10] T. Kinjo, T. Senjyu, N. Urasaki, and H. Fujita, "Output levelling of renevable energy by electric double-layer capacitor applied for energy storage system," *IEEE Trans. Energy Convers.*, vol. 21, no. 1, pp. 221–227, Mar. 2006.
[11] E. D. Castronuovo and J. A. P. Lopes, "On the optimization of the daily operation of a wind-hydro power plant," *IEEE Trans. Power Syst.*, vol. 19, no. 3, pp. 1599–1606, Aug. 2004.
[12] M. Korpaas, A. T. Holen, and R. Hildrum, "Operation and sizing of energy storage for wind power plants in a market system," *Elect. Power Energy Syst.*, vol. 25, pp. 599–606, 2003.
[13] J. P. Barton and D. G. Infield, "A probabilistic method for calculating the usefulness of a store with finite energy capacity for smoothing electricity generation from wind and solar power," *J. Power Sources*, vol. 162, no. 2, pp. 943–948, Nov. 2006.
[14] M. Lange, "On the uncertainty of wind power predictions—Analysis of the forecast accuracy and statistical distribution of errors," *J. Sol. Energy Eng.*, vol. 127, pp. 177–184, 2005.
[15] S. Bofinger, A. Luig, and H. G. Beyer, "Qualification of wind power forecasts," in *Proc. 2002 Global Wind Power Conf. GWPC'02*, Paris, France.
[16] T. S. Nielsen, A. Joensen, H. Madsen, L. Landberg, and G. Giebel, "A new reference for predicting wind power," *Wind Energy*, vol. 1, pp. 29–34, 1998.
[17] H. Madsen, G. Kariniotakis, A. H. Nielsen, T. S. Nielsen, and P. Pinson, "A protocol for standardizing the performance evaluation of short-term wind power prediction models," in *Proc. 2004 Global Wind Power Conf. GWPC'04*, Chicago, IL.
[18] G. C. Canavos, *Applied Probability and Statistical Methods*. Toronto, ON, Canada: Little, Brown, 1984.
[19] G. Giebel, R. Brownsword, and G. Kariniotakis, The State-of-The-Art in Short-Term Prediction of Wind Power, Deliverable 1.1 of ANEMOS project, Contract No.: ENK5-CT-2002-00665.

Hans Bludszuweit was born in Jena, Germany, in 1974. He received the Dipl.Ing. degree in electrical engineering from the Technical University of Ilmenau, Ilmenau, Germany, in 2001 and now he is pursuing the Ph.D. degree at the University of Zaragoza, Zaragoza, Spain.

He spent a year working for the German photovoltaic manufacturers ANTEC Solar GmbH, Arnstadt and First Solar GmbH, Erfurt as a field test engineer. During a year, he joined the hydrogen research group at the Instituto de Investicaciones Eléctricas (IIE), Cuernavaca, Mexico, before joining in 2003 the CIRCE Foundation in Zaragoza as a Ph.D. student. His interests include renewable energy and energy storage in distributed generation systems.

José Antonio Domínguez-Navarro (S'98–A'99–M'04) received the Ph.D. degree in electrical engineering from the University of Zaragoza, Zaragoza, Spain, in 2000.

In 1992, he joined the University of Zaragoza, where he is currently a Lecturer in the Electrical Engineering Department. He has been involved in some research projects related to the optimization of power distribution networks. His current areas of interest are applications of soft computing in electric power systems, power distribution networks planning, electric markets, and metaheuristic optimization.

Andrés Llombart was born in Alcañiz, Spain, in 1970. He received the Engineering and the Ph.D. degree from the University of Zaragoza (UZ), Zaragoza, Spain, in 1994 and 2000, respectively.

Currently, he is a Lecturer in the Electrical Engineering Department at UZ. He also has been the Electrical Division Director at CIRCE Foundation since 2000. His research interests are the area of electronics applied to renewable energies, resource assessment, wind data filtering, and wind farm production control. He has published several papers in the areas of resonant converters, power quality, electrical measurements, and resource assessment. In addition he has participated in three patents related to the wind power production control and measurement systems.